Optimization of copper (II) adsorption onto novel magnetic calcium alginate/maghemite hydrogel beads using response surface methodology

Huayue Zhu, [†,‡] Yongqian Fu, [†] Ru Jiang, [*,†,‡] Jun Yao, [†] Ling Xiao, [‡] Guangming Zeng [*,§]

[†] Laboratory of Resource Utilization and Pollution Control, College of Life Science, Taizhou University, Taizhou, Zhejiang 318000, China

[‡] Key Laboratory for Biomass-Resource Chemistry and Environmental Biotechnology of Hubei Province, Wuhan University, Wuhan, Hubei 430072, China

[§] Key Laboratory of Environmental Biology and Pollution Control, Hunan University, Ministry of Education, Changsha, Hunan 410082, China

*__Corresponding author:__ *Tel.: +86 158 6763 6396; Fax: +86 576 8513 7066*

E-mail address: *jiangru0576@163.com (R. Jiang)*

Postal address: *No.1139, Municipal Government Avenue, Jiaojiang District, Taizhou City, Zhejiang Province, P R China (318000)*

****Co-corresponding author:** *Tel.: +86 731 8822 754; Fax: +86 731 8823 701*

E-mail address: *zgming@hnu.cn (G. Zeng)*

ABSTRACT

Magnetic calcium alginate hydrogel beads (m-CAHBs, 3.4 mm average diameter) composed of maghemite nanoparticles and calcium alginate were prepared and characterized by scanning electron microscopy (SEM) coupled with energy dispersive X-ray analysis (EDX). The response surface methodology was used to model and optimize the adsorption removal of Cu(II) from aqueous solution by m-CAHBs. Adsorption experiments were also carried out to examine the effect of three parameters, such as pH (2.0-6.0), adsorbent dosage (2.0-6.0 g L^{-1}) and initial Cu(II) ion concentration (250-750 mg L^{-1}). Maximum percent removal was attained under the optimum conditions with pH 2.0, 2.0 g L^{-1} adsorbent dosage for 250 mg L^{-1} initial Cu(II) ion concentration. The amount of Cu(II) adsorption after 6 h was recorded as high as 159.24 mg g^{-1} for 500 mg L^{-1} initial Cu(II) ion concentration. The adsorption kinetics indicated that the adsorption process was better described by the pseudo-second-order kinetic model. Desorption experiments indicated that the adsorption mechanism of Cu(II) occurred preferentially more by chelation than by electrostatic interaction. The percent removal of Cu(II) on m-CAHBs could still be maintained at 73 % level at the 5th cycle.

KEYWORDS: Copper(II); Central composite design; Adsorption; Response surface methodology; Optimization

1. INTRODUCTION

Effluents containing Cu(II) with various concentrations are widely discharged from industries such as electroplating, mining and metal plating.[1-2] The presence and accumulation of Cu(II) ions in the aquatic environment not only pose a serious threat to human health, but also have detrimental effects on the aquatic ecosystem.[3] Therefore, it is necessary to remove Cu(II) ions from the waste effluents to meet increasingly stringent environmental quality standards. The main methods used for Cu(II) ions removal from wastewater include chemical precipitation, filtration and adsorption etc.[3-6] Bioadsorption is proved to be a highly effective technique due to the initial cost, simplicity of design and easiness of operation by using natural biomasses, such as shell, rice husk, chitosan, alginate, etc.[3,7-9] Among those biomasses, alginate is a polysaccharide biopolymer composed of (1→4) linked *α-L*-guluronate (G) and *β-D*-mannuronate (M), which has been widely used for the removal of heavy metals and organic dyes from wastewater.[7,10] It shows a strong affinity to metal ions by forming complexes between carboxyl groups of alginate and metal ions. In addition, the gelling properties of its guluronate residues with divalent metallic ions such as Ca^{2+} allow the formation of alginate matrices for hydrogels, beads, pellets and films.[11]

In recent years, much attention has been paid to magnetic assisted adsorption separation technology.[12,13] Magnetic properties could be imparted to bioadsorbents facilitating their trapping from the aqueous solution using a magnetic field compared to the centrifugal methods.[9,14] Magnetite (Fe_3O_4) and maghemite (γ-Fe_2O_3) have been widely used as magnetic materials due to their excellent magnetic properties, chemical stability and biocompatibility.[3,12-16] Recently, many researches have reported about magnetic bioadsorbent or photocatalyst based on calcium alginate and their applications in water treatment.[17-19] However, to our knowledge, there was little

published research on magnetic calcium alginate bioadsorbents applying maghemite (γ-Fe_2O_3) as magnetic source.

In addition, it's well known that adsorption efficiency depends on various experimental factors, such as adsorbent dosage, initial adsorbate concentration, temperature, and pH, etc. Conventional adsorption experiments were usually carried out by varying some experimental factor and keeping the others constants, to determine the influence of each one of the factors.[20] The obvious shortcomings associated with these conventional methods were non-reliability of the results, non-depiction of the combined effect of the independent variables and greater time consumption due to more experiments.[21] Response surface methodology (RSM) is an empirical statistical technique used to evaluate the relationship between a set of controlled experimental factors and observed results. It has been widely used in adsorption processes for the optimization of reaction processes and the evaluation of the relative significance of several parameters in the presence of complex interactions.[22,23] Compared with a one-factor-at-a-time design, which is adopted most frequently in the literature, the experimental design and RSM can effectively reduce experiment runs and the reagents consumption, and facilitate the execution of experiments necessary for the construction of the response surface.

In this study, novel magnetic alginate hydrogel beads (m-CAHBs) composed of magnetic γ-Fe_2O_3 nanoparticles and calcium alginate were prepared and characterized by scanning electron microscopy (SEM) coupled with energy dispersive X-ray analysis (EDX). RSM combined with central composite design (CCD) was used to design and optimize the adsorption process of Cu(II) ions from aqueous solution by the m-CAHBs. Furthermore, the adsorption kinetics was

investigated and adsorption mechanism was proposed. The desorption and reusability of m-CAHBs for Cu(II) ions was also examined.

2. MATERIALS AND METHODS

2.1. Materials

Sodium alginate (20-40 cP, 1% in H_2O (lit.)) was purchased from Sigma-Aldrich (Shanghai) Trading Co., Ltd. Commercially available magnetic γ-Fe_2O_3 nanoparticles (20-30 nm outer diameters, 98 % purity) was obtained from Tongrenweiye Technology Co., Ltd (Shijiazhuang, China). Other chemicals such as copper chloride, sodium hydroxide, hydrochloric acid and calcium chloride were of reagent grade and used without further purification. Double distilled water was used throughout the experiments.

2.2. Preparation of m-CAHBs

The magnetic calcium alginate hydrogel beads (m-CAHBs) were composed of magnetic γ-Fe_2O_3 nanoparticles entrapped by calcium alginate. The mechanism for preparation of m-CAHBs can be illustrated in Fig. 1. About 400 mL of precursor suspension was prepared by mixing 8 g of sodium alginate powder and 4 g of γ-Fe_2O_3 nanoparticles in distilled water. The mixture was vigorously stirred with a mechanical stirrer for 2 h. The viscous suspension containing sodium alginate and maghemite was dropwised through a needle into in a $CaCl_2$ bath (0.1 mol L^{-1}), and thus spherical magnetic alginate hydrogel beads were formed instantaneously. The flow rate was controlled about 20 drops per minute. The beads were cured in $CaCl_2$ solution for 10 h to ensure the complete gelation reaction. Then the hydrogel magnetic beads were collected by a magnet, rinsed three times with double distilled water and kept in a distilled water bath.

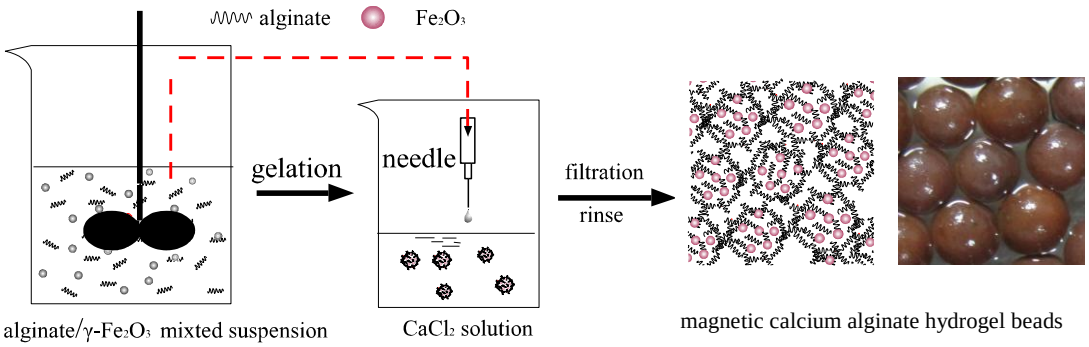

Figure 1. A schematic presentation of the preparation process of m-CAHBs

2.3. Characterization

SEM photographs were taken with Hitachi SX-650 Scanning Microscope (Tokyo, Japan) to examine the morphology and surface structure of the beads at the required magnification at room temperature. The dry beads were deposited on a brass hold and sputtered with a thin coat of gold under vacuum. Acceleration voltage used was 20 kV with the secondary electron image as a detector. An energy dispersive X-ray with a scanning electron microscope (SEM-EDX) was used to quantify the chemical compositions of the m-CAHBs. An IXUS 95 IS digital Cannon camera (Japan) was used to take photos of solution after magnetic separation.

2.4. Batch adsorption experiments

Batch adsorption experiments for Cu(II) ions removal using m-CAHBs were conducted using a thermostatic shaker. A predetermined amount of adsorbent was added to 25 mL solution of known concentration in 100 mL flasks. The solutions were agitated for 6 h at a constant speed of 150 rpm at 30±1 ℃. After the contact time defined by experimental design, the adsorbent was separated by a magnet. All the adsorption experiments were conducted in triplicate.

Percent removal was determined using the following equation:

$$\eta = \frac{(C_0 - C_e)}{C_0} \times 100\,(\%) \tag{1}$$

The amount of Cu(II) ions adsorption on m-CAHBs, q_e (mg g^{-1}), was determined using the

mass balance equation:

$$q_e = \frac{(C_0 - C_e)V}{m} \tag{2}$$

where C_0 and C_e are the initial and final concentrations of Cu(II) ions in mg L^{-1}, V is the volume of the solution in L and m is the mass of dry adsorbent in g.

2.5. Experimental design

Central composite design (CCD), which is widely used form of RSM, was employed in the experimental design procedure. The total number and sequence of experimental runs were determined using Design Expert 8.0.5 software (Stat-Ease, Minneapolis, MN, USA). Adsorbent dosage (X_1), initial solution pH (X_2) and initial copper ion concentration (X_3) were selected as independent input variables. Percent removal (Y_1) and the amount of Cu(II) ions adsorption after 6 h (Y_2) were taken as dependent output response variables of the system. The experimental ranges and the levels of the independent variables for Cu(II) ion removal on m-CAHBs are given in Table S1. Preliminary experiments were performed to determine the extreme values of the variables. The influence of pH was not studied beyond 6.0 due to the formation of precipitate. A total of 20 experiments were employed in the study, including 2^3=8 cube points, 6 replications at the center point and 2×3=6 axial points.

In a system involving three independent variables, the mathematical relationship of the response Y to these variables can be approximated by the quadratic (second-degree) polynomial equation:

$$Y = b_0 + \sum_i^k b_i x_i + \sum_i^k b_{ii} x_i^2 + \sum_i \sum_j b_{ij} x_i x_j + \varepsilon_r \tag{3}$$

where Y is a response variable of removal efficiency; i and j take value from 1 to the number of independent process variables; the b_i values are regression coefficients for linear effects; b_{ii} and b_{ij}

values are the regression coefficients for quadratic effects; x_i and x_j are coded experimental levels of the variables; ε_r is the error of prediction.

Statistical analysis, including the analysis of variance (ANOVA), *t*-test, *F*-test and the determination of the coefficients (R^2), was performed using the software Design-Expert 8.0.5.

3. RESULTS AND DISCUSSION

3.1. Characterization of m-CAHBs

The characterizations of m-CAHBs are shown in Fig. 2. The optical photomicrographs of the wet m-CAHBs illustrated that the whole hydrogel beads had a smooth and dark brown surface due to the presence of maghemite nanoparticles (Fig. 2 a). However, the original color of CAHBs clearly showed white before the introduction of maghemite nanoparticles (Fig. 2 b). The average diameter of the wet m-CAHBs was about 3.41 mm and the size distribution fitted the Gaussian distribution on the whole (Fig. 2 c). The morphology of the dry m-CAHBs was investigated using SEM and corresponding results are shown in Fig.2 d. As can be seen, the dry m-CAHBs are also well shaped spheres with about 1 mm in diameter (Fig. 2 d). Obviously, the size of dry m-CAHBs was much smaller than that of wet m-CAHBs, which was about 3.41 mm (Fig. 2 c). In addition, the surface microstructure of the microspheres was rough (Fig. 2 e), and it can clearly be seen that maghemite nanoparticles has been achieved on the surface of the microspheres. To reveal further the component of m-CAHBs, the energy dispersion spectroscopy (EDS) analysis has been performed on the SEM. The EDS result in Fig. 2 findicated that m-CAHBs were mainly composed of elements C, O, Ca and Fe. The quantitative analysis showed that the weight ratio of C, O, Ca and Fe was 29.91:48.49:7.69:9.96. Therefore, the result of EDS indicated the magnetic maghemite has been existed in the novel calcium alginate hydrogel beads.

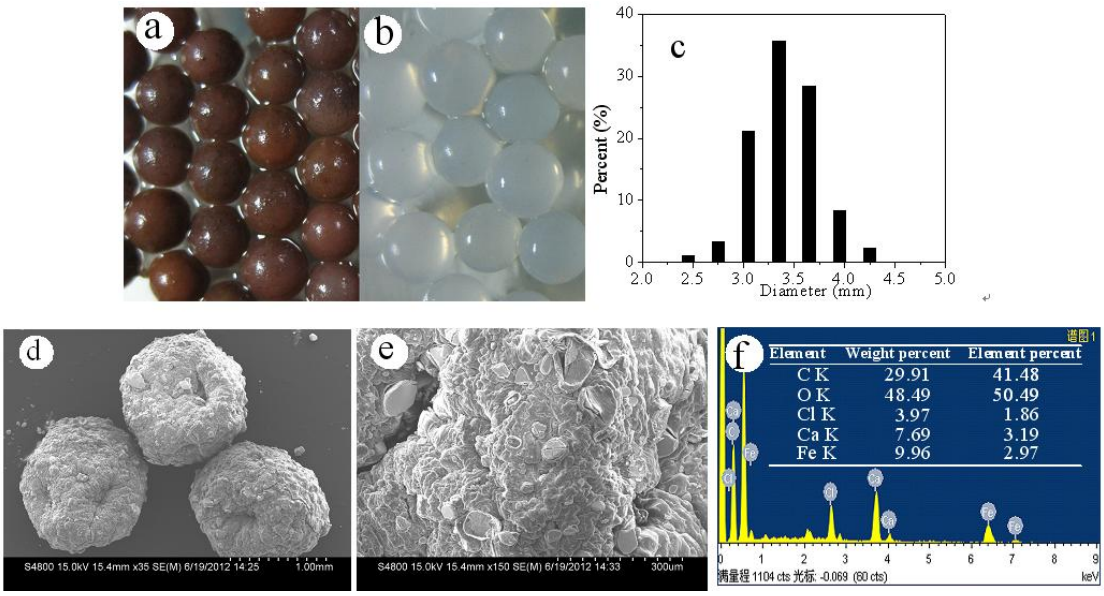

Figure 2. Characterization of the as-prepared m-CAHBs

The magnetic separability of such a magnetic hydrogel beads was tested in water by placing a magnet near the glass, clearly demonstrating the magnetic properties of composite. Fig. 3 showed the magnetic response of m-CAHBs in a magnetic field. As can be seen, the magnetic hydrogel beads could be quickly collected on the side of the cuvette in 10 s and easily removed from the aqueous solution with a magnet. Based on the result, the m-CAHBs will be very advantageous to be used as materials for adsorption and separation.

Figure 3. Photograph of m-CAHBs attracted by a magnet

3.2. CCD model and statistical analysis

The sequence of experiments and summary of the results are given in Table S2. The percent removal and the amount of metal adsorption after 6 h in the fifth and seventh columns represent the average result of three parallel experiments.

Based on these results, empirical relationships between the responses and independent variables in the coded units were obtained and expressed by the following second-order polynomial regression equations:

$$Y_1\,(\%) = 75.68 + 4.29x_1 - 0.40x_2 - 3.58x_3 - 0.33x_1x_2 - 0.31x_1x_3 + 0.089x_2x_3 - 0.23x_1^2 - 3.05x_2^2 + 1.23x_3^2 \quad (4)$$

$$Y_2\,(\text{mg g}^{-1}) = 93.85 - 25.74x_1 - 0.34x_2 + 24.77x_3 - 0.76x_1x_2 - 6.42x_1x_3 + 0.46x_2x_3 + 7.72x_1^2 - 3.76x_2^2 + 0.20x_3^2 \quad (5)$$

The percent removal (Y_1 , %) and amount of metal adsorption (Y_2, mg g^{-1}) have been predicted by Eqs. (4) and (5) and also presented in the sixth and eighth columns of Table 2. It indicates good agreements between the experimental and predicted values. The correlation coefficient (R^2) quantitatively evaluates the correlation between the experimental data and the predicted responses. In this study, the values of the correlation coefficient (R^2=0.9003 for Y_1 and 0.9928 for Y_2), indicating that 90.03 % and 99.28 % of the variability in the response could be explained by the regression models. The adjusted correlation coefficient (adjusted R^2) is a measure of goodness of a fit, but it corrects the R^2 for the sample size and the number of terms in the model by using the degrees of freedom on its computations. If there are many terms in the model and the sample size is not very large, the adjusted R^2 may be noticeably smaller than the R^2 value.[20] Here, the adjusted R^2 values (0.8103 for Y_1 and 0.9864 f for Y_2) are also very high to advocate for a high significance of the models, which ensures a satisfactory adjustment to the polynomial model to the

experimental data. “Adequacy precision” measures the signal to noise ratio. It is reported that a ratio greater than 4 is desirable.[24] The ratio of 10.500 for Y_1 and 40.803 for Y_2 indicates an adequate signal. These two models can be used to navigate the design space.

The observed experimental value versus predicted value displays the real responses’ data plotted against the predicted responses. The regression lines are with high regression coefficients (R>0.95). The experimental data points are well disributed close to a straight line, suggesting an relatively excellent relationship between the experimental and predicted values of the responses, and the underlying assumptions of the above analysis are appropriate.[25]

Analysis of variance (ANOVA) is required to test the significance and the adequacy of the model and is presented in Table S3. The significant of the coefficient term is determined by the value of F and p, and the larger the value of F and the smaller the value of p, the more significant is.[26] The F value of Fischer is obtained by the relationship between the variance due to the regression and the residual variance (F value=S^2_{reg}/S^2_{err}). If the model is a good predictor of the experimental results, F value should be greater than the tabulated value of the F-distribution for a cetain number of degrees of freedom in the model at a level of significance α.[20] F-ratios obtained for percent removal and adsorption capacity, 10.03 and 153.95 respectively, are clearly greater than the value of tabular F value ($F_{0.05(9,10)\ tabular}$=3.02) at the 5 % level, indicating that the treatment differences are highly significant. Prob > F is the probability that all the variation in the results are due to random error,[27] and thus the very low probability values (<0.0001) obtained for both two responses indicate that results are not random and the models is significant. The p is lower than 0.05, suggesting the model is considered to be statistically significant.[28] As shown in Table 2, x_1, x_3 and x_2^2 are significant parameters for percent removal, while x_1, x_3, x_1x_3, x_1^2 and x_2^2

are significant parameters for amount adsorption for Cu(II) adsorption. The other model terms, whose values of *p* value are higher than 0.1000 in Table 2, are not significant. Eliminating those insignificant terms from the regression Eqs.(4) and (5) and refining the model, the above empirical model equations may be simplified as:

$$Y_1\,(\%) = 75.68 + 4.29x_1 - 3.58x_3 - 3.05x_2^2 \quad (6)$$

$$Y_2\,(\text{mg g}^{-1}) = 93.85 - 25.74x_1 + 24.77x_3 - 6.42x_1x_3 + 7.72x_1^2 - 3.76x_2^2 \quad (7)$$

In addition, the adequacy of the models was also evaluated by the residuals (difference between the observed and the predicted response values). Residuals are thought as elements of variation unexplained by the fitted model and then it is expected that they occur according to a normal distribution. Normal probability plots are a suitable graphical method for judging the normality of the residuals.[20,27] The observed residuals were plotted against the expected values, given by a normal distribution (see Fig.S1 (a) and (b)). The approximate straight lines obtained indicate that residuals are normally distributed. Residuals should also presented structureless patterns when plotted against predicted values, showing no increase as the size of the fitted value increases. Trends observed in Fig. S1 (a) and (b) revealed reasonably well-behaved residuals. Based on these plots, the residuals appeared to be randomly scattered.

3.3. Response surface and counter plots

The three-dimensional response surface plots can provide useful information about the behavior of the system within the experimental design, facilitate an examination of the effects of the experimental factors on the responses and contour plots between the factors.[29]

In Fig.4 a, the effect of adsorbent dosage and pH on percent removal is shown at initial Cu(II) concentration of 500 mg L^{-1}. The percent removal increased from 61.61 % to 83.43 % if adsorbent

dosage was increased from 2 g L^{-1} to 6 g L^{-1} keeping initial Cu(II) concentration and pH constant (500 mg L^{-1} and 4.0, respectively). This is expected due to the fact that the higher dosage of m-CAHBs in the solution resulted in greater availability of exchangeable sites for Cu(II) ions. In agreement, as has been shown in Fig.5 (a), the amount of Cu(II) adsorption decreased with the increase of adsorbent dosage. It can be attributed to the reason that an increase in the adsorbent dosage led to unsaturation of the adsorbent sites for constant Cu(II) ions concentration and volume.[30,31]

Fig.4 b represents the effect of adsorbent dosage and initial Cu(II) concentration on the percent removal under the predefined conditions. The percent removal decreased with increase in initial Cu(II) concentration and decrease in adsorbent dosage, reaching a maximum adsorption percent (92.62 %) at initial pH 4.0 and adsorbent dosage of 6 g L^{-1} for initial Cu(II) concentration of 250 mg L^{-1}. An increase in initial Cu(II) concentration led to increase in the amount of metal adsorption on m-CAHBs (Fig.5 b). This increase in loading capacity of the magnetic adsorbent with relation to metal ions concentration is probably due to a high driving force for mass transfer.[30]

Fig. 4 c shows that the percent removal first increased and then decreased with the increase in pH, and increased with the increase in adsorbent dosage. The effect of pH on percent removal may be discussed on the basis of the nature of the chemical interactions of Cu(II) ions with the m-CAHBs. At the lowest pH value of the studied range, i.e. 2.0, the solution is highly acidic in nature. The amino groups ($-NH_2$) were more easily protonated and the carboxylic groups (-COOH) retained their protons, thus reducing the probability of electrostatic binding.[31,32] Consequently, the percentage of metal ion removal is relatively small at lower pH. As pH increased, the reducing

protonation of the amino groups and the increasing dissociation of carboxylic groups could improve the adsorption.

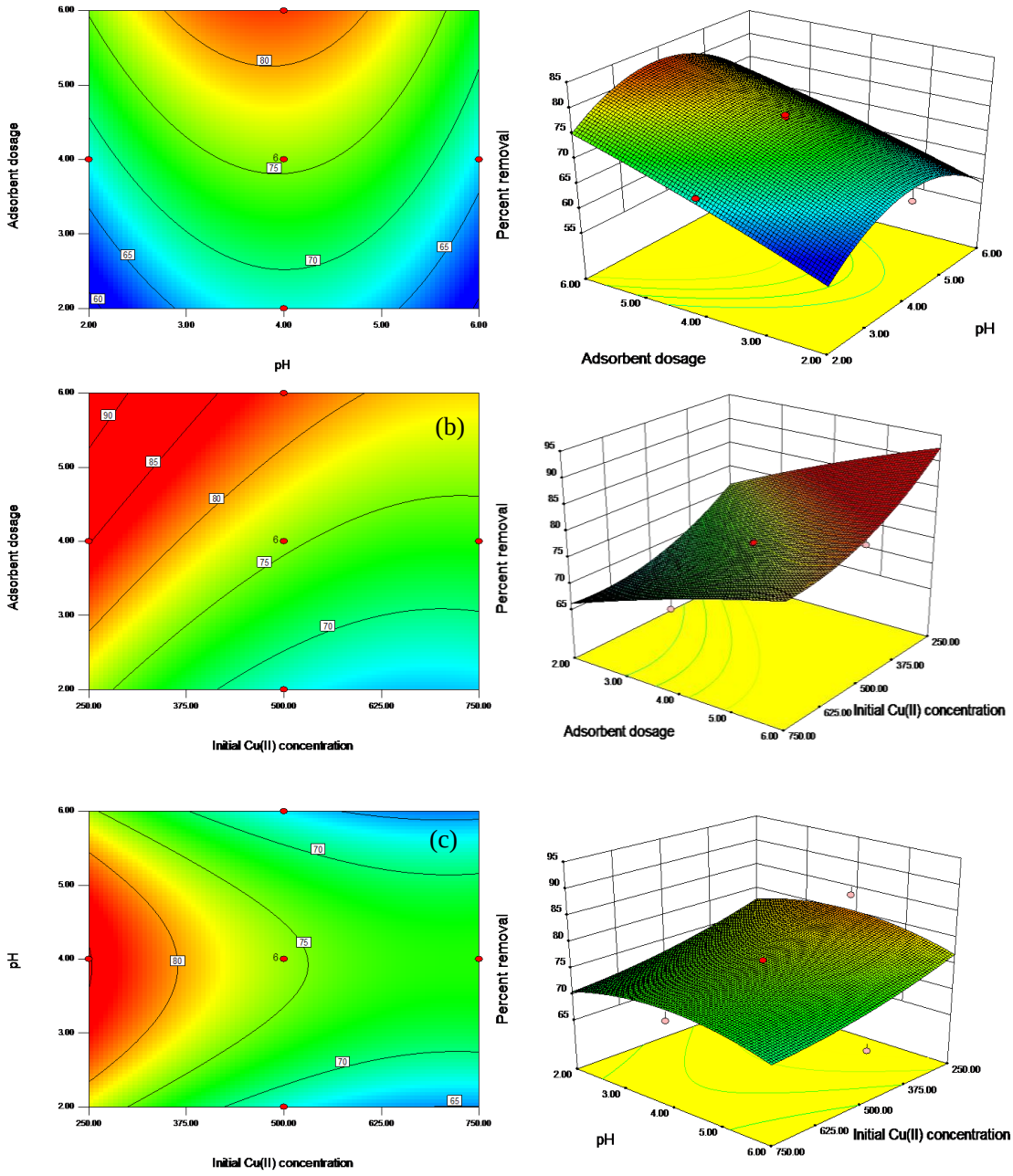

Figure 4. Surface and contour plots for percent removal (%) in uncoded values for t=6 h. (a) X_1 (Adsorbent dosage) and X_2 (pH) in fixed X_3 (Initial Cu(II) concentration) at 500 mg L^{-1}, (b) X_1 (Adsorbent dosage) and X_3 (Initial Cu(II) concentration) in fixed X_2 (pH) at 4, (c) X_2 (pH) and X_3 (Initial Cu(II) concentration) in fixed X_1 (Adsorbent dosage) at 4 g L^{-1}

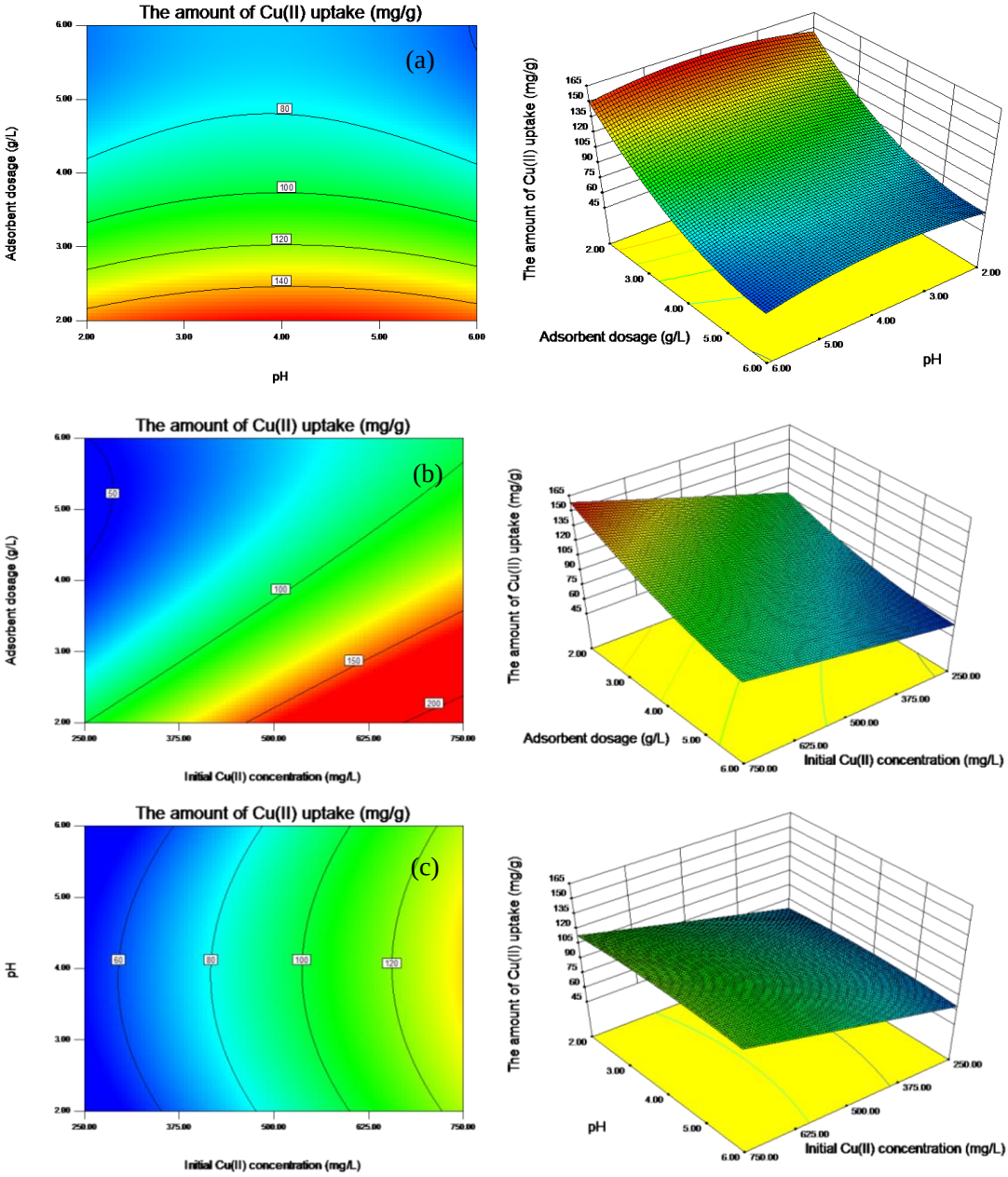

Figure 5. Surface and contour plots for amount of metal adsorption (mg g^{-1}) in uncoded values for t=6 h. (a) X_1 (Adsorbent dosage) and X_2 (pH) in fixed X_3 (Initial Cu(II) concentration) at 500 mg L^{-1}, (b) X_1 (Adsorbent dosage) and X_3 (Initial Cu(II) concentration) in fixed X_2 (pH) at 4, (c) X_2 (pH) and X_3 (Initial Cu(II) concentration) in fixed X_1 (Adsorbent dosage) at 4 mg L^{-1}

3.4. Kinetic study

It is important to be able to predict the rate at which contamination is removed from aqueous solution in order to design an adsorption treatment plant.[20,33] The experimental data was fitted with linearized forms of Lagergren-first-order (Eq.(8)) and pseudo-second-order (Eq.(9)) equations

$$\log(q_e - q_t) = \log q_e - \frac{k_1}{2.303}t \tag{8}$$

$$\frac{t}{q_t} = \frac{1}{k_2 q_e^2} + \frac{t}{q_e} \tag{9}$$

where q_e and q_t are the amount of metal adsorbed (mg g^{-1}) per unit of adsorbent at the equilibrium and at time t, respectively. k_1 is the Lagergren-first-order rate constant (min^{-1}) and k_2 is the pseudo-second-order rate constant of adsorption (g mg^{-1} min^{-1}). The initial adsorption rate (h, mg mg^{-1} min^{-1}) at $t \rightarrow 0$ can be determined from is defined k_2 and q_e values using

$$h = k_2 q_e^2 \tag{10}$$

The kinetic parameters in both two models can be determined from the slopes and the intercepts of linear plots of $\log(q_e\text{-}q_t)\text{-}t$ and $t/q_t\text{-}t$ and summarized in Table 1. Based on the obtained correlation coefficients, adsorption of Cu(II) on m-CAHBs is better described by the pseudo-second order equation. In addition, the experimental value ($q_{e,exp}$) is more closer to the theoretical value ($q_{e,cal}$) calculated from pseudo-second-order model, confirming the validity of that model to the adsorption system. It can be concluded that the main adsorption mechanism of Cu(II) on m-CAHBs is chemical adsorption. The carboxylic (-COOH) and amino ($-NH_2$) groups present on the m-CAHBs was responsible for the binding of Cu(II).

Table 1. Kinetic Parameters for Cu(II) Ions Adsorption by m-CAHBs

	Pseudo-first-order			*Pseudo-second-order*			
$q_{e,exp}$ (mg g^{-1})	k_1 (min^{-1})	$q_{e,cal}$ (mg g^{-1})	R^2	k_2 (g mg^{-1} min^{-1})	$q_{e,cal}$ (mg g^{-1})	R^2	H (mg mg^{-1} min^{-1})

41.915	2.515×10^{-2}	12.559	0.9682	7.14×10^{-2}	41.597	0.9997	12.355

3.5. Desorption

Desorption studies are important since they contribute to elucidate the nature of adsorption process. Additionally, it is necessary to examine the possibility to recover metal ions and to regenerate and recycle the adsorbent. In this study, 0.1 mol L^{-1} EDTA and HCl solutions were used as eluents for adsorbent loaded with Cu(II) ions. Consecutive adsorption-desorption cycles were repeated five times using the same adsorbent in solutions. Desorption values obtained revealed that EDTA was more efficient than HCl because EDTA is a hexadentate chelating agent and is capable of forming a complex with Cu(II) ions much higher (shown in Table S 2), compared to HCl acting as a cation exchanger agent.[34] This also indicated that the adsorption mechanism of Cu(II) occurred preferentially more by chelation than by electrostatic interaction. The percent removal of Cu(II) on m-CAHBs could still be maintained at 73 % level at the 5th cycle (Fig. 7). No significant decrease in the percent removal was observed.

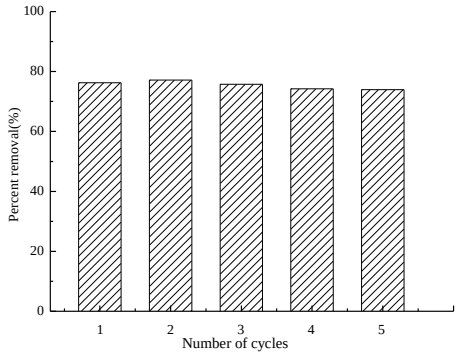

Figure 6. Repeated adsorption of Cu(II) by m-CAHBs. C_0=500 mg L^{-1}, adsorbent dosage = 4 g L^{-1}, pH=5.05, contact time 6 h

3.6. Performance comparison with other adsorbents

The maximum adsorption capacity (q_{max}) of m-CAHBs is listed in Table 2 with literature

values of q_{max} of other adsorbents for Cu(II) adsorption. Weight of dry adsorbent (g) has been used for comparison of q_{max} values (mg g^{-1} dry weight) of all the adsorbents listed in Table 2. The maximum adsorption capacity value obtained in this study for Cu(II) (159.24 mg g^{-1}) was superior to the other adsorbents shown in Table 4. It can be concluded that m-CAHBs is suitable for the removal of Cu(II) from aqueous solutions for its outstanding adsorption capacity.

Table 2. Maximum Adsorption Capacities for Cu(II) Adsorption onto Various Adsorbents

adsorbent	adsorption capacity (mg g^{-1})	ref
chitosan-tripolyphosphate beads	26.06	33
epichlorohydrin cross-linked xanthate chitosan (ECXCs)	43.47	6
Immobilized *Saccharomyces cerevisiae* on the surface of chitosan-coated magnetic nanoparticles (SICCM)	144.9	3
cross-linked magnetic chitosan-isatin Schiff's base resin (CSIS)	103.16	12
chitosan-coated sand	8.18	8
Thiourea-modified magnetic chitosan microspheres	66.7	9
carbon nanotube/calcium alginate composites (CNTs/CA)	67.9	1
calcium alginate encapsulated magnetic sorbent	60	17
magnetic calcium alginate hydrogel beads (m-CAHBs)	159.24	present study

4. CONCLUSION

In the present study, magnetic alginate hydrogel beads (m-CAHBs) composed of magnetic γ-Fe_2O_3 nanoparticles and calcium alginate were used to optimize the adsorptive removal of Cu(II) by applying response surface methodology. The average diameter of m-CAHBs was about 3.41 mm in wet condition. The surface structure of m-CAHBs was analyzed by scanning electron microscopy (SEM) coupled with energy dispersive X-ray analysis (EDX). Maximum percent removal was attained under the optimum conditions with pH 2.0, 2.0 g L^{-1} adsorbent dosage for 250 mg L^{-1} initial Cu(II) ion concentration. The amount of Cu(II) adsorption after 6 h was

recorded as high as 159.24 mg g^{-1} for 500 mg L^{-1} initial Cu(II) ion concentration. The data indicated that the adsorption process was better described by the pseudo-second-order kinetics, suggesting the chemical adsorption in nature. The percent removal of Cu(II) on m-CAHBs could still be maintained at 73 % level at the 5th cycle. The m-CAHBs is suitable for the removal of Cu(II) from aqueous solutions for its outstanding adsorption capacity and excellent magnetic response.

AUTHOR INFORMATION

Corresponding Author

Tel.: +86 158 6763 6396. Fax: +86 576 8513 7066.

E-mail address: jiangru0576@163.com (R. Jiang)

Notes

The authors declare no competing financial interest.

ACKNOWLEDGEMENTS

Financial support from the National Natural Science Foundation of China (No. 21007044, 51208331) and the Professional Development Foundation of a Visiting Scholar from Education Department of Zhejiang Province (No. FX201205) are gratefully acknowledged.

SUPPORTING INFORMATION

Table S1. Experimental Range and Levels of the Independent Variables

Table S2. The 3-Factor Central Composite Design Matrix and Values of Response

Table S3. ANOVA of the Selected Quadratic Model for Cu(II) Adsorption on m-CAHBs

Table S4 Desorption of copper (II) from m-CAHBs using different desorbing agent.

Figure S1. Residual plots for copper (II) ions adsorption on m-CAHBs of percent removal (a) and the amount of metal adsorption (b)

This material is available free of charge via the Internet at http://pubs.acs.org.

REFERENCE

(1) Li, Y.; Liu, F.; Xia, B.; Du, Q.; Zhang, P.; Wang, D.; Wang, Z.; Xia, Y. Removal of copper from aqueous solution by carbon nanotube/calcium alginate composites. *J. Hazard. Mater.* **2010**, *177*(1-3), 876.

(2) Wan Ngah, W. S.; Teong, L. C.; Toh, R. H.; Hanafiah, M. A. K. M. Utilization of chitosan–zeolite composite in the removal of Cu(II) from aqueous solution: Adsorption, desorption and fixed bed column studies. *Chem. Eng. J.* **2012**, *209*, 46.

(3) Peng, Q.; Liu, Y.; Zeng, G.; Xu, W.; Yang, C.; Zhang, J. Biosorption of copper(II) by immobilizing Saccharomyces cerevisiae on the surface of chitosan–coated magnetic nanoparticles from aqueous solution. *J. Hazard. Mater.* **2010**, *177*(1-3), 676.

(4) González, M. M. J.; Rodríguez, M. A.; Luque, S. A.; Álvarez, J. R. Recovery of heavy metals from metal industry waste waters by chemical precipitation and nanofiltration. *Desalination* **2006**, *200*(1), 742.

(5) Muthukrishnan. M.; Guha, B. K. Heavy metal separation by using surface modified nanofiltration membrane. *Desalination* **2006**, *200*, 351.

(6) Kannamba, B.; Reddy, K. L.; AppaRao, B. V. Removal of Cu(II) from aqueous solutions using chemically modified chitosan. *J. Hazard. Mater.* **2010**, *175*(1-3), 939.

(7) Papageorgiou, S. K.; Katsaros, F. K.; Kouvelos, E. P.; Kanellopoulos, N. K. Prediction of binary adsorption isotherms of Cu^{2+}, Cd^{2+} and Pb^{2+} on calcium alginate beads from single adsorption data. J. *Hazard. Mater.* **2009**, *162*(2-3), 1347.

(8) Wan, M. W.; Kan, C. C.; Rogel, B. D.; Dalida, M. L. P. Adsorption of copper (II) and lead (II) ions from aqueous solution on chitosan–coated sand. *Carbohydr. Polym.* **2010**, *80*(3), 891.

(9) Zhou, L.; Wang, Y.; Liu, Z.; Huang, Q. Characteristics of equilibrium, kinetics studies for adsorption of Hg(II), Cu(II), and Ni(II) ions by thiourea–modified magnetic chitosan microspheres. *J. Hazard. Mater.* **2009**, *161*(2-3), 995.

(10) Wan Ngah, W. S.; Fatinathan, S. Adsorption of Cu(II) ions in aqueous solution using chitosan beads, chitosan–GLA beads and chitosan–alginate beads. *Chem. Eng. J.* **2008**, *143*(1-3), 62.

(11) Kim, T.Y.; Jin, H. J.; Park, S. S.; Kim, S. J.; Cho, S. Y. Adsorption equilibrium of copper ion and phenol by powdered activated carbon, alginate bead and alginate–activated carbon bead. *J. Ind. Eng. Chem.* **2008**, *14*(6), 714.

(12) Monier, M.; Ayad, D. M.; Wei, Y.; Sarhan, A. A. Adsorption of Cu(II), Co(II), and Ni(II) ions by modified magnetic chitosan chelating resin. *J. Hazard. Mater.* **2010**, *177*(1-3), 962.

(13) Zhu, H. Y.; Fu, Y. Q.; Jiang, R.; Yao, J.; Xiao, L.; Zeng, G. M. Novel magnetic chitosan/poly (vinyl alcohol) hydrogel beads: Preparation, characterization and application for adsorption of dye from aqueous solution. *Bioresour. Technol.* **2012**, *105*, 24.

(14) Zhu, H. Y.; Fu,Y. Q.; Jiang, R.; Jiang, J. H.; Xiao, L.; Zeng, G. M.; Zhao, S. L.; Wang,Y. Adsorption removal of congo red onto magnetic cellulose/Fe_3O_4/activated carbon composite: Equilibrium, kinetic and thermodynamic studies. *Chem. Eng. J.* **2011**, *173*(2), 494.

(15) Fan, L.; Luo, C.; Sun, M.; Li, X.; Lu, F.; Qiu, H. Preparation of novel magnetic chitosan/graphene oxide composite as effective adsorbents toward methylene blue. *Bioresour. Technol.* **2012**, *114*, 703.

(16) Wang, Y.; Wang, X.; Luo, G.; Dai, Y. Adsorption of bovin serum albumin (BSA) onto the magnetic chitosan nanoparticles prepared by a microemulsion system. *Bioresour. Technol.* **2008**, *99*(9), 3881.

(17) Lim, S. F.; Zheng, Y. M.; Zou, S. W.; Chen, J. P. Characterization of copper adsorption onto an alginate encapsulated magnetic sorbent by a combined FT–IR, XPS, and mathematical modeling study. *Environ. Sci. Technol.* **2008**, *42*(7), 2551.

(18) Lim, S. F.; Zheng, Y. M.; Zou, S. W.; Chen, J. P. Removal of copper by calcium alginate encapsulated magnetic sorbent. *Chem. Eng. J.* **2009**, *152*(2-3), 509.

(19) Zhu, H. Y.; Jiang, R.; Xiao, L.; Cao, C. H.; Zeng, G. M. CdS nanocrystals/TiO_2/crosslinked chitosan composite: Facile preparation, characterization and adsorption-photocatalytic properties. *App. Surf. Sci.* **2013**, *273*, 661

(20) Santos, C. R. S.; Boaventura, R. A. R. Adsorption modeling of textile dyes by sepiolite. *Appl. Clay Sci.* **2008**, *42*(1-2), 137.

(21) Chatterjee, S.; Kumar, A.; Basu, S.; Dutta, S. Application of response surface methodology for methylene blue dye removal from aqueous solution using low cost adsorbent. *Chem. Eng. J.* **2012**, *181-182*(1), 289.

(22) Garg, U. K.; Kaur, M. P.; Sud, D.; Garg, V. K. Removal of nickel (II) from aqueous solution by adsorption on agricultural waste biomass using a response surface methodological approach. *Bioresour. Technol.* **2008**, *99*(5), 1325.

(23) Lü, J.; Zhou, P. Optimization of microwave-assisted $FeCl_3$ pretreatment conditions of rice straw and utilization of *Trichoderma viride* and *Bacillus pumilus* for production of reducing sugars. *Bioresour. Technol.* **2011**, *102*(13), 6966.

(24) Muthukumar, M.; Mohan, D.; Rajendran, M. Optimization of mix proportions of mineral aggregates using Box Behnken design of experiments. *Cement Concrete Compos.* **2003**, *25*(7), 751.

(25) Liu,Y.; Wang, J.; Zheng, Y.; Wang, A. Adsorption of methylene blue by kapok fiber treated by sodium chlorite optimized with response surface methodology. *Chem. Eng. J.* **2012**, *184*(1), 248.

(26) Amini, M.; Younesi, H.; Bahramifar, N.; Lorestani, A. A. Z.; Ghorbani, F.; Daneshi, A.; Sharifzadeh, M. Application of response surface methodology for optimization of lead biosorption in an aqueous solution by Aspergillus niger. *J. Hazard. Mater.* **2008**, *154*(1-3), 694.

(27) Fathinia, M.; Khataee, A. R.; Zarei, M.; Aber, S. Comparative photocatalytic degradation of two dyes on immobilized TiO_2 nanoparticles: effect of dye molecular structure and response surface approach. *J. Mol. Cataly A: Chem.* **2010**, *333*(1-2), 73.

(28) Kim, H. K.; Kim, J. G.; Cho, J. D.; Hong, J. W. Optimization and characterization of UV–curable adhesives for optical communications by response surface methodology. *Polym. Test.* **2003**, *22*(8), 899.

(29) Panesar, P. S. Application of response surface methodology in the permeabilisation of yeast cells for lactose hydrolysis. *Biochem. Eng. J.* **2008**, *39*(1), 91.

(30) Aydın, H.; Bulut, Y.; Yerlikaya, C. Removal of copper (II) from aqueous solution by adsorption onto low–cost adsorbents. *J. Environ. Manage.* **2008**, *87*(1), 37.

(31) Vijaya, Y.; Popuri, S. R.; Boddu, V. M.; Krishnaiah, A. Modified chitosan and calcium alginate biopolymer sorbents for removal of nickel (II) through adsorption. *Carbohydr. Polym.* **2008**, *72*(2), 261.

(32) Bajpai, J.; Shrivastava, R.; Bajpai, A. K. Dynamic and equilibrium studies on adsorption of Cr(VI) ions onto binary bio–polymeric beads of cross linked alginate and gelatin. *Colloids Surf., A* **2004**, *236*(1-3), 81.

(33) Wan Ngah, W. S.; Fatinathan, S. Adsorption characterization of Pb(II) and Cu(II) ions onto chitosan–tripolyphosphate beads: Kinetic, equilibrium and thermodynamic studies. *J. Environ. Manage.* **2010**, *91*(4), 958.

(34) Wan Ngah, W. S.; Kamari, A.; Koay, Y. J. Equilibrium and kinetics studies of adsorption of copper (II) on chitosan and chitosan/PVA beads. *Int. J. Biol. Macromol.* **2004**, *34*(3), 155.

Table Captions

Table 1 Experimental range and levels of the independent variables

Table 2 ANOVA of the selected quadratic model for Cu(II) adsorption on m-CAHBs

Table 3 Kinetic parameters for Cu(II) ions adsorption by m-CAHBs

Table 4 Maximum adsorption capacities for Cu(II) adsorption onto various adsorbents

Figure Captions

Figure 1. A schematic presentation of the preparation process of m-CAHBs

Figure 2. Characterization of the as-prepared m-CAHBs

Figure 3. Photograph of m-CAHBs attracted by a magnet

Figure 4. Residual plots for copper (II) ions adsorption on m-CAHBs of percent removal (a) and the amount of metal adsorption (b)

Figure 5. Surface and contour plots for percent removal (%) in uncoded values for t=6 h. (a) X_1 (Adsorbent dosage) and X_2 (pH) in fixed X_3 (Initial Cu(II) concentration) at 500 mg L^{-1}, (b) X_1 (Adsorbent dosage) and X_3 (Initial Cu(II) concentration) in fixed X_2 (pH) at 4, (c) X_2 (pH) and X_3 (Initial Cu(II) concentration) in fixed X_1 (Adsorbent dosage) at 4 g L^{-1}

Figure 6. Surface and contour plots for amount of metal adsorption (mg g^{-1}) in uncoded values for t=6 h. (a) X_1 (Adsorbent dosage) and X_2 (pH) in fixed X_3 (Initial Cu(II) concentration) at 500 mg L^{-1}, (b) X_1 (Adsorbent dosage) and X_3 (Initial Cu(II) concentration) in fixed X_2 (pH) at 4, (c) X_2 (pH) and X_3 (Initial Cu(II) concentration) in fixed X_1 (Adsorbent dosage) at 4 mg L^{-1}

Figure 7. Repeated adsorption of Cu(II) by m-CAHBs. C_0=500 mg/L, adsorbent dosage = 4 g/L, pH=5.05, contact time 6h.